ACS OMEGA

http://pubs.acs.org/journal/acsodf

Article

Anion Receptor Enhanced Li Ion Transportation for High-Performance Lithium Metal Batteries

Zhixin Wang,[#] Zhipeng Cai,[#] Meinan Liu, Fuliang Xu, and Fangmin Ye*

Cite This: *ACS Omega* 2023, 8, 16411−16418

Read Online

ACCESS | Metrics & More | Article Recommendations | Supporting Information

ABSTRACT: High-potential lithium metal batteries (LMBs) are still facing many challenges, such as the growth of lithium (Li) dendrites and resultant safety hazards, low-rate capabilities, etc. To this end, electrolyte engineering is believed to be a feasible strategy and interests many researchers. In this work, a novel gel polymer electrolyte membrane, which is composed of polyethyleneimine (PEI)/poly(vinylidene fluoride-*co*-hexafluoropropylene) (PVDF-HFP) cross-linked membrane and electrolyte (PPCM GPE), is prepared successfully. Due to the fact that the amine groups on PEI molecular chains can provide the rich anion receptors and strongly pin the anions of electrolytes and thus confine the movement of anions, our designed PPCM GPE owns a high Li^+ transference number (0.70) and finally contributes to the uniform Li^+ deposition and inhibits the growth of Li dendrites. In addition, the cells with PPCM GPE as a separator behave the impressive electrochemical performances, i.e., a low overpotential and an ultralong and stable cycling performance in Li||Li cells, a low overvoltage of about 34 mV after a stable cycling for 400 h even at a high current density of 5 mA/cm^2, and, in Li||LFP full batteries, a specific capacity of 78 mAh/g after 250 cycles at a 5 C rate. These excellent results suggest a potential application of our PPCM GPE in developing high-energy-density LMBs.

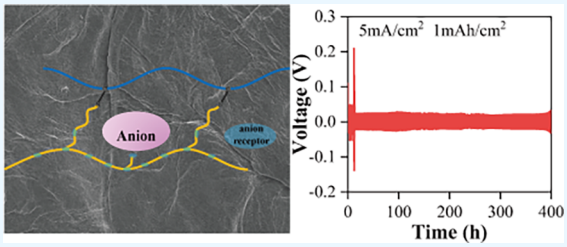

1. INTRODUCTION

With the burgeoning demand for high-energy-density batteries powering portable devices, new energy vehicles, and so on, lithium metal batteries (LMBs), which are based on Li metal anodes with a high theoretical specific capacity (3860 mAh/g) and an extraordinarily low electrochemical potential (−3.04 V vs standard hydrogen electrode), become one of the alternatives of high specific energy storage devices.[1] However, the irreversible Li consumption because of the complex interfacial reaction between the active Li and the electrolyte and the possible growth of Li dendrites because of the uneven deposition of Li decrease the battery capacity and shorten the battery life and, more importantly, cause terrible safety hazards. Therefore, the practical application of LMBs is still retarded.[2−7]

To develop the safe and high-energy-density LMBs, a variety of strategies including modification of the Li metal anode, separator, and electrolyte were presented in the past 1920s.[8−10] Among them, the polymer electrolytes used in LMBs, because of their potentially excellent mechanical properties, high safety, and stable electrochemical performances, are regarded as one of the feasible approaches.[11−13] Unfortunately, the polymer electrolytes usually behave a low ionic conductivity and a small Li^+ transference number due to the disordered Li^+ transportation and strong Li^+ solvation. Low ionic conductivity can to a large extent affect the rate performance of LMBs, so fast charge/discharge LMBs will be difficultly realized. Furthermore, a small Li^+ transference number for electrolytes usually contributed to an uneven Li deposition, which probably causes the growth of Li dendrites and finally shortens the lifetime of batteries.[14] Therefore, regulation of polymer electrolytes with a high ionic conductivity and Li^+ transference number is very meaningful. To this end, Cui and coworkers[15] reported a cross-linked poly(tetrahydrofuran) by introducing a loosened O−Li coordination to lead to an ionic conductivity of 1.2×10^{-4} S/cm and a Li^+ transference number of 0.53 at room temperature, finally improving the electrochemical performance of batteries. Liu and coworkers[16] used a copolymer polysiloxane grafted by bifunctional groups of the cyclic propylene carbonate (PC) and combed poly(ethylene oxide) (PEO) on the side chain of polysiloxane to realize that the ionic conductivity can be tuned by adjusting the ratio of PC/PEO and realize an ionic conductivity of 1.55×10^{-4} S/cm at room temperature. Very recently, acrylonitrile- and vinylene carbonate-induced poly(vinylene carbonate-acrylonitrile) gel polymer electrolyte (PVN-GPE) realizes the strong polarity of the cyano groups and ester groups of GPE, which finally increases the Li^+ transference numbers.[17]

Traditionally, the movement of anions usually dominates in the polymer electrolyte,[18] which results in a small Li^+

Received: February 24, 2023
Accepted: April 13, 2023
Published: April 26, 2023

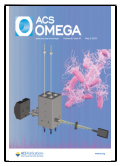

transference number. Therefore, to retard the movement of anions, e.g., hexafluorophosphate anion (PF_6^-) and bis-(trifluoromethane)sulfonimide anion ($TFSI^-$), and thus to increase the Li^+ transference number, introduction of anion receptors is believed to be another feasible method,[19] which was demonstrated by an anion-trapping supermolecular component incorporation into PEO-LiX,[20] the urea calix arene (C4A) and poly(ethylene glycol)-borate ester (B-PEG) into the cross-linked Si doped-poly(ethylene glycol) (Si-PEG),[21] and a polydopamine and 1,3-dioxolane (PDA-DOL) copolymerization-enhanced interaction between the $-NH_2-$ and $-NH-$ groups of PDA and DOL and $TFSI^-$.[22] Nonetheless, the design of the functional polymer electrolyte is still facing some challenges, such as mechanical properties, flexibility, and ionic conductivity.

Herein, a polyethyleneimine (PEI)/poly(vinylidene fluoride-*co*-hexafluoropropylene) (PVDF-HFP) cross-linked polymer membrane (PPCM) by introducing PEI into PVDF-HFP and the resultant PPCM-based gel polymer electrolyte (PPCM GPE) were successfully designed. Due to the cross-linking of PEI with PVDF-HFP and the novel fabrication method, our designed PPCMs have a gradient pore structure, ordered channels, and a uniform distribution of PEI on the PPCM. Especially, due to the affinity of $-NH_2$ and electrolyte anions, PPCM GPE possessed a Li^+ transference number of 0.70 at room temperature, which largely boosts the rate capability and life of batteries. For Li||Li symmetric cells, the cells with PPCM GPE had a very low and stable overpotential at different current densities (1, 2, and 5 mA/cm^2); even at 5 mA/cm^2, the overvoltage of PPCM-based cells still can remain stable within 34 mV for more than 400 h. Also, for a practical Li||LFP full cell, the cells with PPCM GPE had a remarkable reversibility and a better rate performance, i.e., a specific capacity of 106 mAh/g after 400 cycles at a 1 C rate with a stable high Coulombic efficiency (CE) of above 99.5%; at a higher rate of 5 C, the initial specific capacity reached 116 mAh/g, and the initial CE is as high as 96.8%, and after 250 cycles, a specific capacity of 80 mAh/g with a CE of above 97% can be still delivered. The ex situ SEM results reveal the uniform Li^+ deposition on the surface of Li metal for the PPCM GPE-based cells. Our excellent results suggest a feasible route to boost the practical application of LMBs.

2. EXPERIMENTAL SECTION

2.1. Chemicals and Materials. PVDF-HFP was purchased from Sigma-Aldrich (average Mw = 400,000, average Mn = 130,000). PEI was bought from Aladdin Reagent (Shanghai) Co., Ltd. (Mw = 10,000, 99%). Dimethyl sulfoxide (DMSO) and ethanol were purchased from Shanghai Macklin Biochemical Co., Ltd. $LiFePO_4$ powder was supplied from Shenzhen Kejing Technology Co., Ltd. PVDF was supplied from Arkema (HSV900). Acetylene black was purchased from Suzhou Sinero Technology Co., Ltd. *N*-Methylpyrrolidone (NMP) and Li metal were purchased from Suzhou Dodo Chemistry Technology Co., Ltd. The two electrolytes were composed of 1 M Li hexafluorophosphate ($LiPF_6$) in ethylene carbonate (EC)/dimethyl carbonate (DMC) (1/1) (v/v) and 1 M bis(trifluoromethane)sulfonimide Li salt (LiTFSI) in methoxymethane (DME)/1,3-dioxolane (DOL) (1/1) (v/v) with 1% $LiNO_3$, respectively, which were supplied from Dodo Chemistry Technology Co., Ltd.

2.2. Preparation of the PPCM/PVDF-HFP Membrane and GPE. In a typical experiment, the PEI was first dissolved into DMSO solvent to obtain a solution with a concentration of 100 mg/mL. Then, PVDF-HFP and DMSO with a mass ratio of 3:17 were mixed at a water bath of 60 °C and a stir of 6 h to form a PVDF-HFP solution. Then, the solution was transferred to a water bath of 40 °C for 10 min, and then PEI solution was added quickly (PEI:PVDF-HFP mass ratio = 1:20). Next, the mixture was coated on a glass plate (100 × 90 × 1 mm) by a doctor blade. And the glass plate was placed on a low-temperature copper block kept in a freezer at −80 °C for more than 2 h (100 mm × 90 mm × 50 mm) and was pushed slowly and uniformly to obtain a frozen film. After that, the frozen glass plate was immersed in a low-temperature ethanol (<0 °C) for 12 h to replace the DMSO in the film, and the soaked film was peeled off from the glass plate and placed in an oven at 60 °C for vacuum drying for 12 h Finally, the dried film was cut into 18 mm wafer in diameter to obtain the final PPCM. Using the same method, the PVDF-HFP membrane was prepared and used as a reference.

The gel electrolyte was obtained by immersing the as-prepared membranes in EC/DMC (1/1) (v/v) at 1.0 M Li hexafluorophosphate ($LiPF_6$) for about 15 min and was followed by removing the excess liquid electrolyte from the membrane surface with a dust-free paper.

2.3. Preparation of the LFP Cathode. LFP cathode electrodes were composed of LFP powder, PVDF, and acetylene black (their mass ratio: 8:1:1). The detailed prepared process is as follows. First, PVDF was dissolved to NMP solvent and was stirred at room temperature for 6 h to form a solution. Then, the LFP powder and acetylene black were mixed together in a mortar and then were dispersed to the above PVDF solution and stirred for 12 h to make the evenly mixed slurry. The well-mixed slurry was coated on the aluminum foil by a doctor blade with a thickness of 100 μm and then placed in an oven at 60 °C for vacuum drying for 24 h. Finally, the aluminum foil coated by the active material was cut into 12 mm cathode plates in diameter. The loading mass of LFP on the cathode electrode is about 3−4 mg/cm^2.

2.4. Structural Characterization. The morphology and microstructure of PPCM were observed by a field emission scanning electron microscope (FESEM, Hitachi S-4800) under a 3 kV acceleration voltage. Before the test, the sample of section view was torn by two tweezers after freezing in liquid nitrogen. At the same time, the mapping spectrum of nitrogen distribution was recorded under an accelerating voltage of 10 kV. The Fourier transform infrared (FTIR) spectra were measured on an infrared spectrometer (Thermo Scientific, Nicolet iS50 series) with a wavenumber range of 600 to 4000 cm^{-1}. Tensile tests were carried out on a Legendary 2366 INSTRON with a 50 N load cell at a tensile speed of 5 mm/min. The stretched sample of the PEI/PVDF-HFP membrane was made into 16 mm × 10 mm × 0.08 mm cuboid, and the stretched sample of the PVDF-HFP membrane was made into 16 mm × 10 mm × 0.1 mm cuboid.

2.5. Electrochemical Measurements. The ionic conductivities were tested by AC impedance spectroscopy using a CHI760E electrochemical workstation (CH Instruments, China). The symmetrical battery that PPCM was sandwiched between two stainless steel (SS) electrodes was assembled, and the AC impedance was measured over a frequency range of 0.1 Hz to 100 kHz with an amplitude of 10 mV. The ionic conductivity (σ) was calculated by eq 1 at room temperature:

$$\sigma = d/(R_b \times S) \quad (1)$$

https://doi.org/10.1021/acsomega.3c01258
ACS Omega 2023, 8, 16411−16418

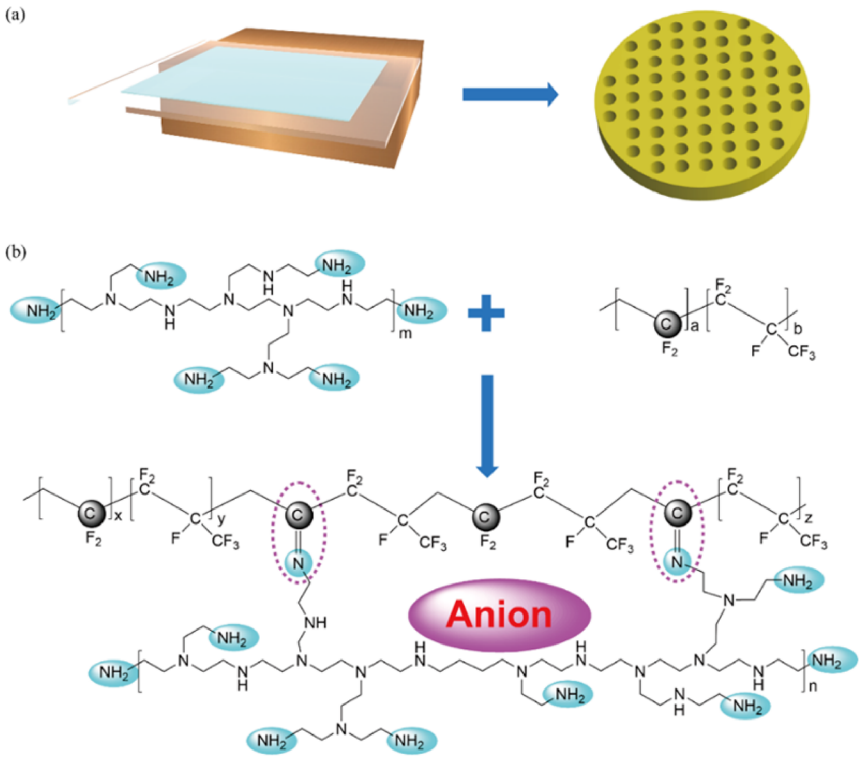

Figure 1. (a) Schematic fabrication process of PPCM; (b) possible formation mechanism of the PPCM cross-linked network structure and the interaction between the PPCM and the electrolyte anion.

where d represents the thickness of the membrane, S represents the effective area of the membrane, and R_b is the ohmic resistance measured from the impedance spectrum.

The Li^+ transference number (t_{Li^+}) was deduced by DC polarization combined with AC impedance using a CHI760E electrochemical workstation (CH Instruments, China). t_{Li^+} was measured by eq 2 at room temperature:

$$t_{Li^+} = \frac{I_{ss}(\Delta V - I_0 R_0)}{I_0(\Delta V - I_{ss}R_{ss})} \quad (2)$$

where ΔV is the applied polarization voltage (10 mV), I_0 and I_{ss} are the initial current and steady-state current, respectively, and R_0 and R_{ss} are the initial interfacial resistance and steady-state interfacial resistance, respectively.

The liquid electrolyte uptake was evaluated by calculating the change rate of weight of the PPCM and PVDF-HFP membrane before and after absorbing the electrolyte. The detailed formula of the electrolyte uptake is based on eq 3:

$$r = \frac{m - m_0}{m_0} \times 100\% \quad (3)$$

where r is the liquid absorption rate, m_0 is the initial mass of the membrane, and m is the mass of the membrane after absorbing the liquid electrolyte and removing the excess electrolyte on the surface.

The electrochemical performance of the coin cells was tested using a battery testing system (Wuhan LANHE CT2001A). The Li||Li symmetric cells were composed of two Li plates with a diameter of 15.6 mm and a thickness of 0.45 mm and 60 μL of liquid electrolyte (1.0 M $LiPF_6$ in EC:DEC 1:1 vol %). The coin cells were tested, adopting a capacity density of 1 mAh/cm^2 and the current densities of 1, 2, and 5 mA/cm^2, respectively. The Li||LFP full cells were composed of 80 μL of liquid electrolyte (1.0 M LiTFSI in DME:DOL 1:1 vol % with 1.0 wt % $LiNO_3$) using the Li plate as the negative electrode and the prepared LFP cathode piece as the positive electrode. The cycle performance of the Li||LFP full cells was tested at the rates of 1 C (1 C = 170 mA/g), 2 C, and 5 C between 2.0 and 4.0 V, respectively. All batteries were tested with a standard coin cell (LIR2025) assembled in an argon-filled glovebox (H_2O or $O_2 \leq$ 1.0 ppm).

3. RESULTS AND DISCUSSION

Figure 1a shows the schematic fabrication process of PPCMs via a freeze-casting method.[23] Our design is based on the following supports. First, poly(vinylidene fluoride) (PVDF) has good chemical and electrochemical stability and high dielectric constant ε (~8.4) due to its strong polar group C−F bond.[24,25] Second, the copolymerization unit of hexafluoropropylene (HFP) can break the regularity of the PVDF macromolecular chain and thus decrease its crystallinity.[26,27] Third, the liquid electrolyte filled in PPCMs is prone to interact with the amorphous part of PVDF to form a gel polymer electrolyte (PPCM GPE), which further promotes the formation of a more adherent and stable interface between the GPE and the Li metal surface.[28−32] Therefore, for introduction of PEI into PVDF-HFP, on the one hand, the primary amine groups of PEI have a strong nucleophilicity and a strong interaction with the C−F bond of PVDF to form a cross-linked network structure, which can reduce the crystallinity of PPCM. The lower crystallinity for PPCM can be further verified by XRD and DSC (Figure S1). It can be found that the intensity of the diffraction peak of XRD for the PPCM membrane is much lower than that of the PVDF-HFP membrane in the same peak position. Meanwhile, DSC curves show that the PPCM membrane has a lower heat absorption peak than the

https://doi.org/10.1021/acsomega.3c01258
ACS Omega 2023, 8, 16411−16418

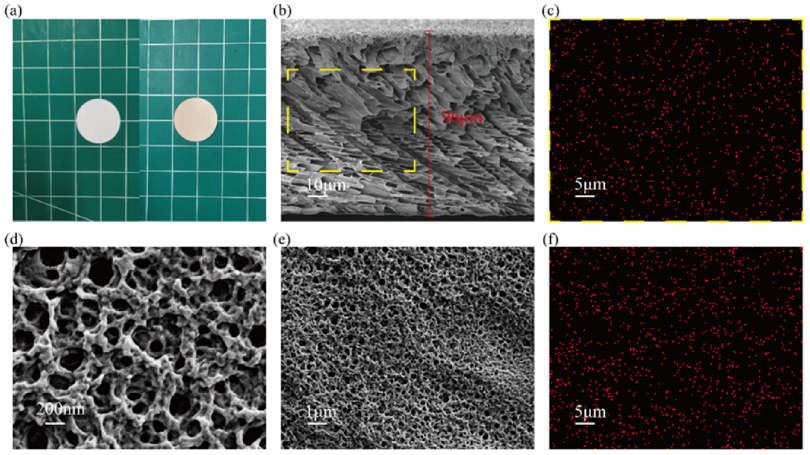

Figure 2. (a) Photograph for the PVDF-HFP membrane (left) and PPCM (right); (b) cross-sectional SEM image for PPCM; (e) surface SEM image of PPCM and (d) a magnified SEM surface for PPCM; (c, f) mappings of the nitrogen element for the PPCM cross section and surface, respectively.

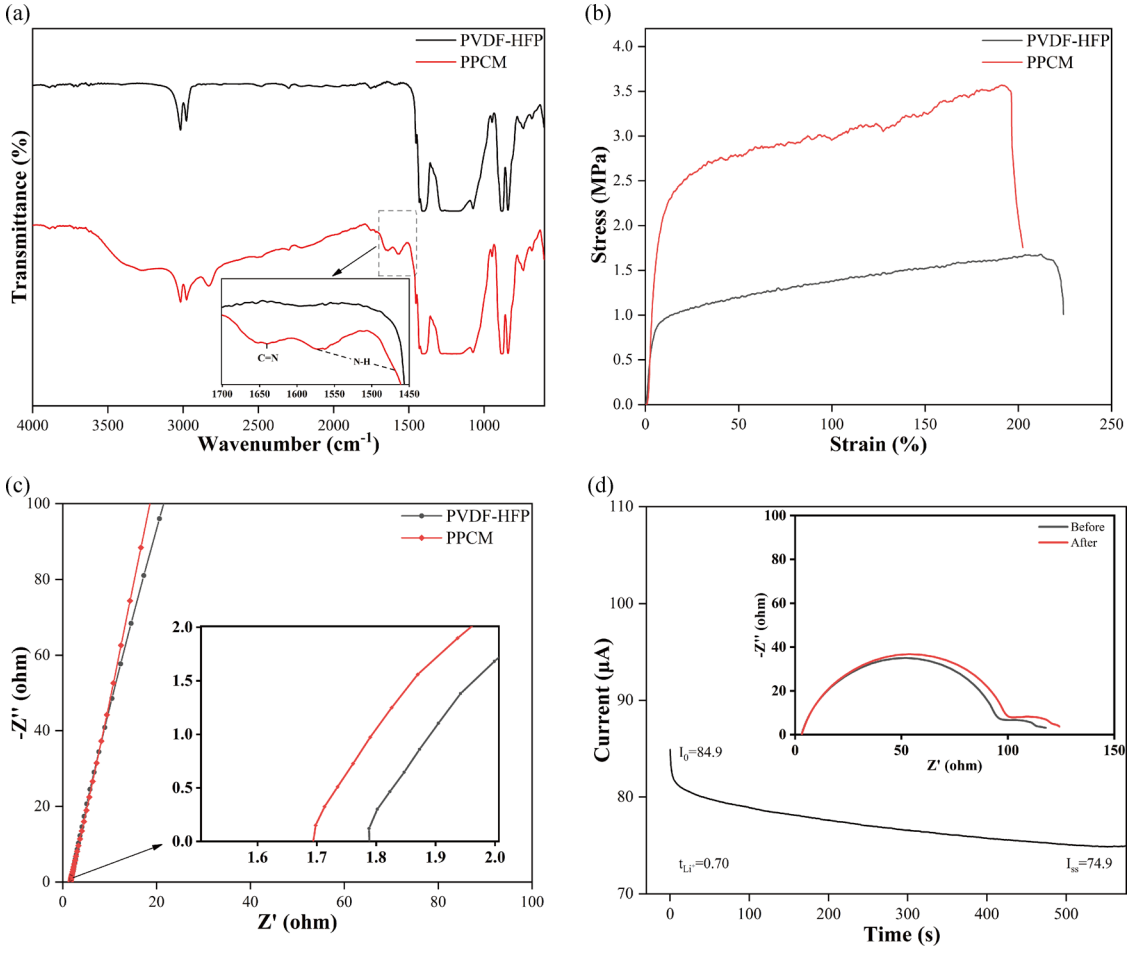

Figure 3. (a) FTIR spectra of PVDF-HFP and PPCM membranes; (b) stress−strain curves of PVDF-HFP and PPCM membranes; (c) Nyquist plots of SS/electrolyte/SS cells with PVDF-HFP GPE and PPCM GPE; (d) chronoamperometry curves with a polarization voltage of 10 mV (the insets displayed the EIS plot before and after polarization) of the PPCM GPE cell.

PVDF-HFP membrane, which is probably ascribed to the destruction of the regularity of the PVDF-HFP molecular chain structure by PEI, also demonstrating the same conclusion. On the other hand, the PEI molecular chain contains a great number of amine groups (e.g., primary, secondary, and tertiary amines), which can act as anion receptors to trap anions in the electrolyte and thus limit the movement of anions (Figure 1b). Both of them largely improve the ionic conductivity and Li^+ transfer number of PVDF-HFP GPE and finally realize a high performance of LMBs.

To reveal the morphology and microstructure of our prepared PPCM, SEM and elementary mapping were collected

https://doi.org/10.1021/acsomega.3c01258
ACS Omega 2023, 8, 16411−16418

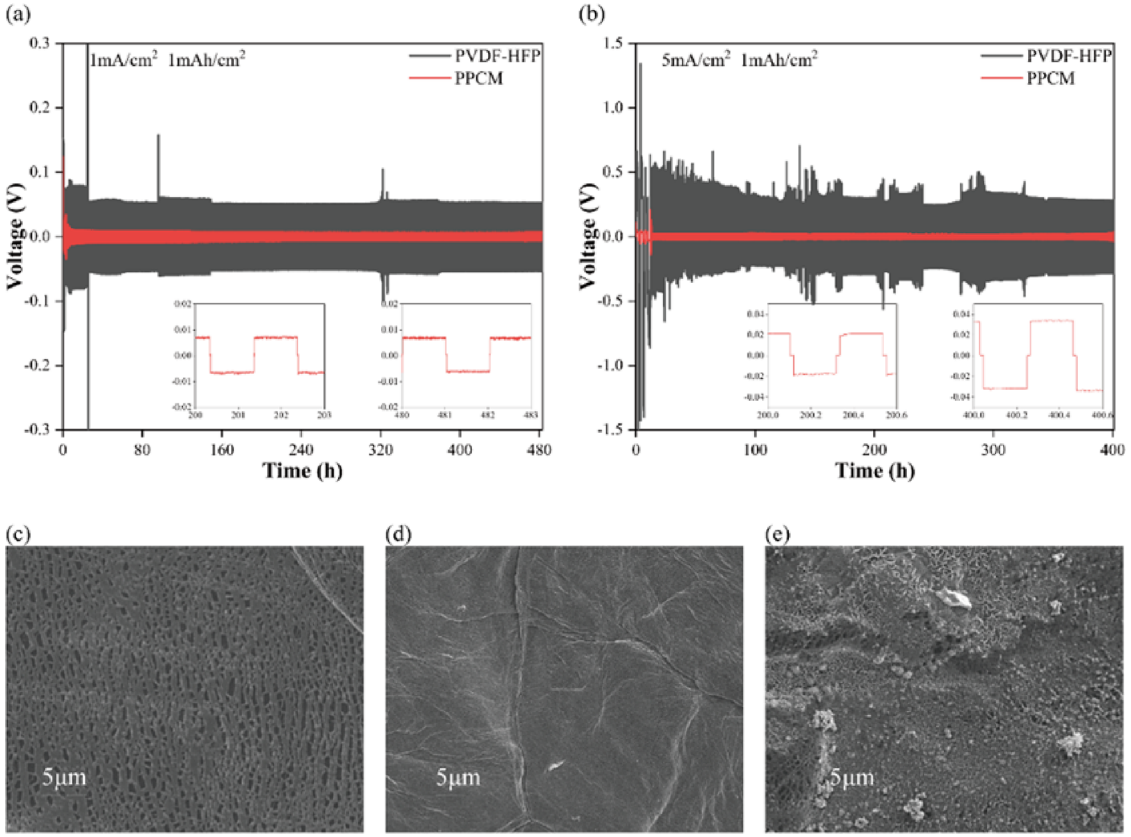

Figure 4. (a) Voltage−time curves of symmetric cells with PVDF-HFP GPE and PPCM GPE when measured at 1 mA/cm^2 with 1 mAh/cm^2; (b) voltage−time curves of symmetric cells with PVDF-HFP GPE and PPCM GPE when measured at 5 mA/cm^2 with 1 mAh/cm^2; (c) SEM images of the new Li plate; (d, e) SEM images of the Li plate of the PPCM GPE cell and PVDF-HFP GPE cell, cycled at 0.5 mA/cm^2 with 1 mAh/cm^2 for 400 h, respectively.

and are shown in Figure 2. Figure 2a shows the photographs of PVDF-HFP and PPCM membranes, respectively. It can be clearly observed that the PVDF-HFP membrane (left) appears pure white, while the PPCM (right) appears pale yellow, which indicates a uniform polymerization of the PVDF-HFP matrix with PEI. The cross-sectional SEM image of PPCM shown in Figure 2b indicates a loose porous structure and a thickness of around 90 μm. Interestingly, an ordered micron-sized channel can be clearly observed, which is in agreement with the reported results.[23] These ordered channels can be expected to shorten the Li transport path and thus increase the ionic conductivity. Also, a thin layer with nano-sized pores on the top surface can be more clearly seen on the surface of PPCM shown in Figure 2e. A magnified SEM image shown in Figure 2d revealed the fine and relatively uniform nano-sized channels, and the pore diameter of the channels is about 200 nm, which is probably conducive to improve the Li^+ transportation.

The similar structure and morphology can be also observed in the PVDF-HFP membrane shown in Figure S2. To further evaluate the effectiveness of PEI cross-linked with PVDF-HFP, the elementary mapping for the nitrogen element was collected and is shown in Figure 2c,f. The uniform distribution of the N element in PVDF-HFP observed from cross-sectional and surface mappings solidly demonstrated that PEI effectively interacted with the PVDF-HFP polymer.

To further dig the interaction mechanism of PVDF-HFP and PEI, the FTIR spectra of the PPCM and PVDF-HFP membrane were collected, respectively. It is well-known that the C−F bond of PVDF-HFP has strong polarity, while the primary amine group ($-NH_2$) on PEI molecular chains is nucleophilic. Therefore, based on Figure 3a, it can be inferred that the C−F bonds easily cross-link with the primary amine to form C=N bonds by a combination of hydrogen and fluoride and their FTIR spectrum. Also, a broad peak observed at the position of 3400−3100 cm^{-1} belongs to the unreacted primary amine stretching vibration peak, and the two other peaks at 2930 and 2830 cm^{-1} should owe to the stretching vibration peaks of the C−H bond of PEI. The peaks shifted toward lower wavenumbers possibly due to the interaction of hydrogen bonds. The previously reported results concluded that the peak at 1640 cm^{-1} should be the C=N bond,[31−33] meaning an effective cross-linking between C−F bonds and the primary amines in our PPCM. In addition, the peaks at 1572 and 1470 cm^{-1} for the bending vibration peaks of the N−H bonds of primary and secondary amines, respectively, also support the cross-linking reaction between PEI and PVDF-HFP. In addition, the optical photographs of PVDF-HFP solution and PPCM gel (Figure S3) further suggest a cross-linking reaction between PEI and PVDF-HFP. At the same time, the cross-linked network structure of PPCM increases the absorption rate of the liquid electrolyte (Table S1), which means more free volume for PPCM than that of PVDF-HFP, which is beneficial to the Li^+ transportation and the formation of the uniform solid electrolyte interface (SEI).

The mechanical performance was also analyzed by stress−strain curves of our PPCMs measured by the tensile test, and the tested results are shown in Figure 3b. As seen, the

https://doi.org/10.1021/acsomega.3c01258
ACS Omega 2023, 8, 16411−16418

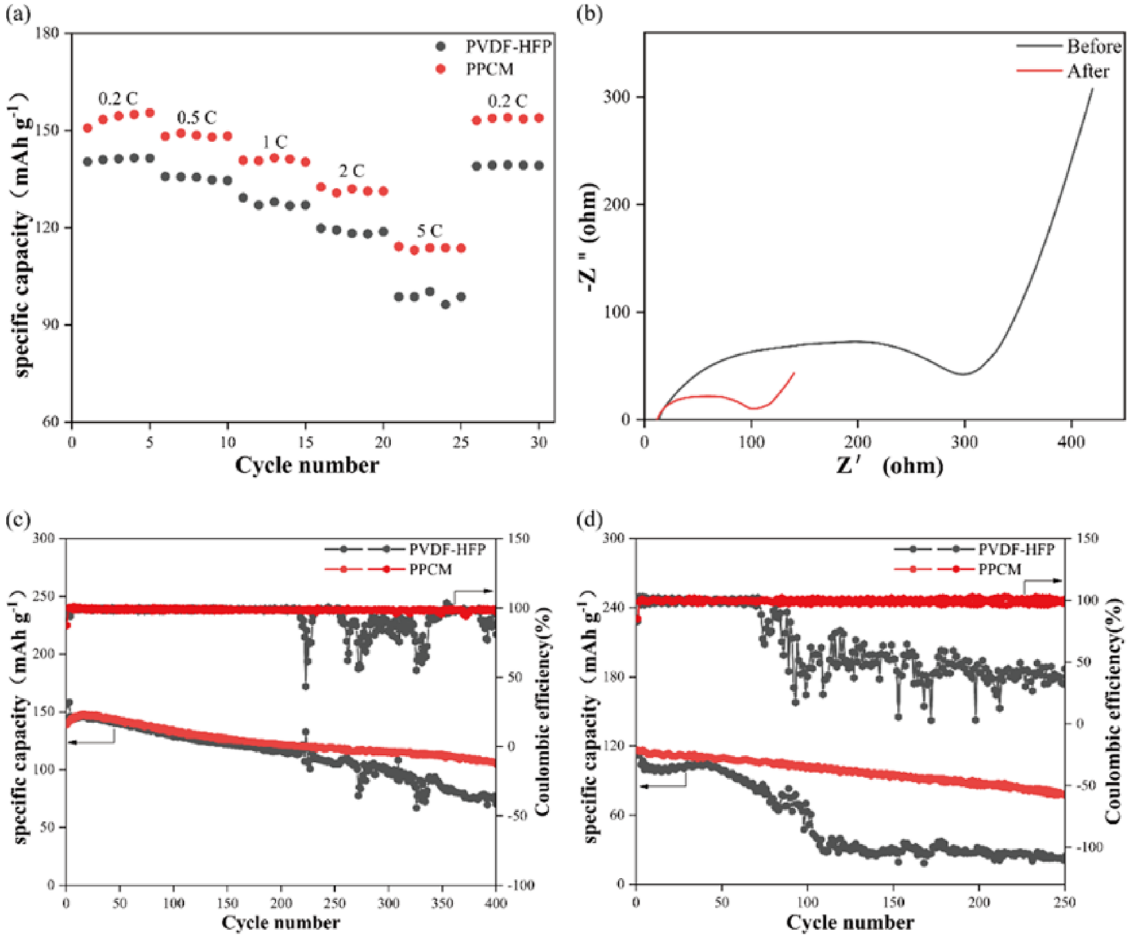

Figure 5. (a) Rate performance of Li||LFP full cells of PVDF-HFP GPE and PPCM GPE; (b) Nyquist plots of Li||LFP full cells of PPCM GPE before and after the rate performance test; (c) discharge capacity and CE of Li||LFP cells of PVDF-HFP GPE and PPCM GPE cycling at 1 C; (d) discharge capacity and CE of Li||LFP cells of PVDF-HFP GPE and PPCM GPE cycling at 5 C.

elongation at break of our PPCM can reach 190%, slightly lower than that of the PVDF-HFP membrane (210%), which is able to resist volume changes during battery operation. However, the maximum tensile strength of PPCM can arrive at 3.57 MPa, much higher than that of PVDF-HFP (about 1.67 MPa), which is originated from the semicrystalline structure of PVDF-HFP and its cross-linking with PEI. The high tensile strength is beneficial to physically inhibit the growth of Li dendrites upon cycling, finally improving the safety of LMBs.

To evaluate the positive function of the PEI additive on improving conductivity and Li^+ transference number, the SS/electrolyte/SS symmetric cells were assembled and the data collected by AC impedance spectroscopy were used to determine the ionic conductivity. According to Figure 3c, the ionic conductivities of PPCM and PVDF-HFP GPE are estimated to be about 2.94×10^{-3} and 2.22×10^{-3} S/cm, respectively. The improved ionic conductivity is probably contributed by broken molecular chains in the crystalline part of PVDF-HFP and reduction of the crystallinity of PPCM and the increase of free volume because of the cross-linked network structure of PPCM.[17−21] In addition, the Li^+ transference number was obtained by using the Li/electrolyte/Li symmetric cells by DC polarization combined with AC impedance, and the result is shown in Figure 3d. Based on the data, the Li^+ transference number can be estimated to be 0.70, which is larger than that of PVDF-HFP (0.53, shown in Figure S4). This improved value should attribute to the amine groups (primary amine, secondary amine, and tertiary amine groups) in the PEI molecular chain, which act as anion receptors to restrict the movement of anions in the cross-linked network of PPCM, thus reducing the interaction of anions with Li^+. A schematic diagram shown in Figure S5 reveals the interaction between anions and PEI. At the same time, Li^+ possibly performs transition motion along with polar bonds freely, which also led to the improvement of the Li^+ transference number.[34] A high Li^+ transference number can effectively suppress the generation of interfacial polarization, which is beneficial to more uniform Li deposition, improving electrochemical performance of LMBs.[19,35]

Based on the novel structures and physical properties aforementioned, the cells with PPCM GPE are expected to display an excellent performance. First, the interfacial stability between the electrolyte and the Li metal was revealed by Li||Li symmetric cells, and the data collected by using the different current densities with a same charge/discharge capacity density of 1 mAh/cm^2 are shown in Figure 4. As seen in Figure 4a, the symmetric cells for PVDF-HFP GPE can last for 480 h at a current density of 1 mA/cm^2 and show a stable overvoltage of 60 mV, indicating a relatively stable interface between PVDF-HFP GPE and Li metal. However, the cell for the PPCM GPE cell shows an ultralow and a very stable initial overvoltage of 7 mV within tested 480 h, indicating a more stable SEI and fast

https://doi.org/10.1021/acsomega.3c01258
ACS Omega 2023, 8, 16411−16418

kinetics for plating/stripping of Li. In addition, the interface stability of the PPCM GPE cell is also better than that of the PP separator (Figure S6). The excellent performance for PPCM GPE can be further supported by a higher current intensity of 2 mA/cm^2 (Figure S7). More surprisingly, even at a current density of 5 mA/cm^2 (Figure 4b), an overvoltage of 22 mV for cells with PPCM GPE after 200 h and 34 mV after 400 h can be realized, while the cells with PVDF-HFP behaves a highly fluctuate plating/stripping process and a much higher overpotential. These excellent performances for PPCM are in agreement with our expectation and support our inference that the anion acceptor from PEI can effectively limit the movement of $TFSI^-$ and lead to the uniform Li deposition, finally enhancing the electrochemical performance of LMBs. A more stable interface induced by the PPCM GPE can also be demonstrated by an ex situ observed surface morphology of Li metal from a cycled cell (Figure 4c,d and Figure S8). Compared with the original Li plate with a flat surface and some observed voids, the surface morphology of Li metal after a cycling of 400 h for PPCM GPE is a ripple-like structure, indicating a ripple-like Li deposition and a relatively flat surface.

On the contrary, the surface of the cycled Li metal for PVDF-HFP GPE shown in Figure 4e appears some undulations and grooves and some little Li dendrites. Furthermore, the components of the SEI layer on the cycled Li metal for PPCM by XPS (Figure S9) suggest that the surface of the SEI layer of Li metal contains Li_2CO_3, LiF, $TFSI^-$, and other inorganic substances.

The potential application of our PPCM GPE in LMBs with LFP as cathodes was also evaluated. First, the rate performance was conducted in turn at rates of 0.2, 0.5, 1, 2, and 5 C. It could be found that the discharge specific capacity for PPCM GPE cells was obviously higher than that of PVDF-HFP GPE cells at the same rates (Figure 5a). Especially at a high rate, the capacity retention rate of PPCM is higher as the rising rate, indicating a better reversibility for PPCM GPE.

When the applied current density returns to 0.2 C, the discharge capacity for PPCM GPE-based cells can go back to the previous value and the capacity retention rate is as high as 99.9%, further proving a more stable interface for PPCM-based cells. The AC impedance carried out by using the PPCM GPE cells before and after the rate test, respectively, supports our results (Figure 5b). It can be found that the interface impedance value for PPCM GPE has a large decrease from the original 300 ohm to 100 after being cycled. For a long cycling test of Li‖LFP cells at a 1 C rate, the initial capacities of the PVDF-HFP GPE cell and PPCM GPE cell were basically the same (Figure 5c). However, the discharge capacity also decreased rapidly and the CE for the PVDF-HFP GPE cell began to fluctuate violently after 218 cycles; on the contrary, the discharge capacity for the PPCM GPE cell can still be kept at 106 mAh/g at 400 cycles. Similarly, the cycling stability and specific capacity of the cell with PPCM GPE are also better than those of the PP separator (Figure S10). More interestingly, the excellent performance at a 5 C rate for PPCM is significantly better than that of the cells for PVDF-HFP (Figure 5d). The CE and specific capacity of the PVDF-HFP cell decayed violently after 73 cycles. However, an initial capacity of 116 mAh/g for the PPCM and a highly stable CE of about 97% can be realized within the rest cycles. These impressive results are consistent with the rate test and symmetric cell test reflected. Therefore, our PPCM designed by introducing PEI to cross-link with PVDF-HFP can effectively inhibit the growth of Li dendrites and boost the rate performance of LMBs.

4. CONCLUSIONS

In summary, PEI was successfully introduced into the PVDF-HFP matrix to prepare a PPCM with a cross-linked network structure. Benefiting from the amine groups of PPCM and a novel cross-linked structure, a high Li^+ transference number of 0.70 can be achieved. Due to the enhanced ionic conductivity and Li^+ transference number, our assembled cells with PPCM GPE show impressive results and exhibit a potential practical application for LMBs, such as Li/PPCM/LFP full cells. Constructing anion receptor-rich porous polymer membranes with a gradient pore distribution is a feasible route for developing high-safety and high-rate LMBs.

■ ASSOCIATED CONTENT

Supporting Information

The Supporting Information is available free of charge at https://pubs.acs.org/doi/10.1021/acsomega.3c01258.

XRD patterns; SEM images; absorption rate of the liquid electrolyte; $I-T$ curves; schematic; XPS spectra of the Li metal surface; and some additional electrochemical characterizations (PDF)

■ AUTHOR INFORMATION

Corresponding Author

Fangmin Ye − *Key Laboratory of Optical Field Manipulation of Zhejiang Province, Department of Physics, Zhejiang Sci-Tech University, Hangzhou, Zhejiang 310018, P. R. China;* orcid.org/0000-0001-6595-0881; Email: fmye2013@sinano.ac.cn

Authors

Zhixin Wang − *Key Laboratory of Optical Field Manipulation of Zhejiang Province, Department of Physics, Zhejiang Sci-Tech University, Hangzhou, Zhejiang 310018, P. R. China*

Zhipeng Cai − *Key Laboratory of Optical Field Manipulation of Zhejiang Province, Department of Physics, Zhejiang Sci-Tech University, Hangzhou, Zhejiang 310018, P. R. China*

Meinan Liu − *i-Lab, Suzhou Institute of Nano-Tech and Nano-Bionics, Chinese Academy of Sciences, Suzhou, Jiangsu 215123, China;* orcid.org/0000-0003-2552-1091

Fuliang Xu − *Key Laboratory of Optical Field Manipulation of Zhejiang Province, Department of Physics, Zhejiang Sci-Tech University, Hangzhou, Zhejiang 310018, P. R. China*

Complete contact information is available at: https://pubs.acs.org/10.1021/acsomega.3c01258

Author Contributions

#Z.W. and Z.C. contributed equally. All authors approve the final version of the manuscript.

Notes

The authors declare no competing financial interest.

■ ACKNOWLEDGMENTS

This work was supported by the National Natural Science Foundation of China (22075313) and the Science Foundation of Zhejiang Sci-Tech University (18062299-Y).

REFERENCES

(1) Tarascon, J.; Armand, M. Issues and challenges facing rechargeable lithium batteries. *Nature* **2001**, *414*, 359−367.
(2) Cheng, X.; Peng, H.; Huang, J.; Zhang, R.; Zhao, C.; Zhang, Q. Dual-Phase Lithium Metal Anode Containing a Polysulfide-Induced Solid Electrolyte Interphase and Nanostructured Graphene Framework for Lithium-Sulfur Batteries. *ACS Nano* **2015**, *9*, 6373−6382.
(3) Cheng, X.; Hou, T.; Zhang, R.; Peng, H.; Zhao, C.; Huang, J.; Zhang, Q. Dendrite-Free Lithium Deposition Induced by Uniformly Distributed Lithium Ions for Efficient Lithium Metal Batteries. *Adv. Mater.* **2016**, *28*, 2888−2895.
(4) Yu, X.; Manthiram, A. Electrode−electrolyte interfaces in lithium-based batteries. *Energy & Environmental Science. Energy Environ. Sci.* **2018**, *11*, 527−543.
(5) Peled, E. The Electrochemical Behavior of Alkali and Alkaline Earth Metals in Nonaqueous Battery Systems-The Solid Electrolyte Interphase Model. *J. Electrochem. Soc.* **1979**, *126*, 2047−2051.
(6) Yang, C.; Yin, Y.; Zhang, S.; Li, N.; Guo, Y. Accommodating lithium into 3D current collectors with a submicron skeleton towards long-life lithium metal anodes. *Nat. Commun.* **2015**, *6*, 8058.
(7) Sawada, Y.; Dougherty, A.; Gollub, J. Dendritic and Fractal Patterns in Electrolytic Metal Deposits. *Phys. Rev. Lett.* **1986**, *56*, 1260−1263.
(8) Kang, D.; Hart, N.; Koh, J.; Ma, L.; Liang, W.; Xu, J.; Sardar, S.; Lemmon, J. Rearrange SEI with artificial organic layer for stable lithium metal anode. *Energy Storage Mater.* **2020**, *24*, 618−625.
(9) Krauskopf, T.; Dippel, R.; Hartmann, H.; Peppler, K.; Mogwitz, B.; Richter, F.; Zeier, W.; Janek, J. Lithium-Metal Growth Kinetics on LLZO Garnet-Type Solid Electrolytes. *Joule* **2019**, *3*, 2030−2049.
(10) Sun, B.; Zhang, Q.; Xu, W.; Zhao, R.; Zhu, H.; Lv, W.; Li, X.; Yang, N. Lithium-Metal Growth Kinetics on LLZO Garnet-Type Solid Electrolytes. *Nano Energy* **2022**, *94*, No. 106937.
(11) Jiang, H.; Han, X.; Du, X.; Chen, Z.; Lu, C.; Li, X.; Zhang, H.; Zhao, J.; Han, P.; Cui, G. A Permselective Polymer Electrolyte with Anion Solvation Regulation Enabling Long-Cycle Dual-Ion Battery. *Adv. Mater.* **2022**, *34*, 2108665.
(12) Almazrou, Y.; Kyu, T. Electrochemical Performance of Highly Ion-Conductive Polymer Electrolyte Membranes Based on Polyoxide-tetrathiol Conetwork for Lithium Metal Batteries. *ACS Appl. Polym. Mater.* **2022**, *4*, 9417−9429.
(13) Zhao, Y.; Tenhaeff, W. Thermally and Oxidatively Stable Polymer Electrolyte for Lithium Batteries Enabled by Phthalate Plasticization. *ACS Appl. Polym. Mater.* **2020**, *2*, 80−90.
(14) Niu, C.; Liu, J.; Chen, G.; Liu, C.; Qian, T.; Zhang, J.; Cao, B.; Shang, W.; Chen, Y.; Han, J.; Du, J.; Chen, Y. Anion-regulated solid polymer electrolyte enhances the stable deposition of lithium ion for lithium metal batteries. *J. Power Sources* **2019**, *417*, 70−75.
(15) Mackanic, D.; Michaels, W.; Lee, M.; Feng, D.; Lopez, J.; Qin, J.; Cui, Y.; Bao, Z. Crosslinked Poly(tetrahydrofuran) as a Loosely Coordinating Polymer Electrolyte. *Adv. Energy Mater.* **2018**, *8*, 1800703.
(16) Li, J.; Lin, Y.; Yao, H.; Yuan, C.; Liu, J. Tuning Thin-Film Electrolyte for Lithium Battery by Grafting Cyclic Carbonate and Combed Poly(ethylene oxide) on Polysiloxane. *ChemSusChem* **2014**, *7*, 1901−1908.
(17) Wang, P.; Chai, J.; Zhang, Z.; Zhang, H.; Ma, Y.; Xu, G.; Du, H.; Liu, T.; Li, G.; Cui, G. An intricately designed poly(vinylene carbonate-acrylonitrile) copolymer electrolyte enables 5 V lithium batteries. *J. Mater. Chem. A* **2019**, *7*, 5295−5304.
(18) Zhao, Y.; Wang, L.; Zhou, Y.; Liang, Z.; Tavajohi, N.; Li, B.; Li, T. Solid Polymer Electrolytes with High Conductivity and Transference Number of Li Ions for Li-Based Rechargeable Batteries. *Adv. Sci.* **2021**, *8*, 2003675.
(19) Zhou, Q.; Ma, J.; Dong, S.; Li, X.; Cui, G. Intermolecular Chemistry in Solid Polymer Electrolytes for High-Energy-Density Lithium Batteries. *Adv. Mater.* **2019**, *31*, 1902029.
(20) Blazejczyk, A.; Wieczorek, W.; Kovarsky, R.; Golodnitsky, D.; Peled, E.; Scanlon, L.; Appetecchi, G.; Scrosati, B. Novel Solid Polymer Electrolytes with Single Lithium-Ion Transport. *J. Electrochem. Soc.* **2004**, *151*, A1762.
(21) Li, D.; Ji, X.; Gong, X.; Tsai, F.; Zhang, Q.; Yao, L.; Jiang, T.; Li, Y.; Shi, H.; Luan, S.; Shi, D. The synergistic effect of poly(ethylene glycol)-borate ester on the electrochemical performance of all solid state Si doped-poly(ethylene glycol) hybrid polymer electrolyte for lithium ion battery. *J. Power Sources* **2019**, *423*, 349−357.
(22) Chen, D.; Zhu, M.; Kang, P.; Zhu, T.; Yuan, H.; Lan, J.; Yang, X.; Sui, G. Self-Enhancing Gel Polymer Electrolyte by In Situ Construction for Enabling Safe Lithium Metal Battery. *Adv. Sci.* **2022**, *9*, 2103663.
(23) Li, L.; Wang, M.; Wang, J.; Ye, F.; Wang, S.; Xu, Y.; Liu, J.; Xu, G.; Zhang, Y.; Yan, C.; Medhekar, V.; Liu, M.; Zhang, Y. Asymmetric gel polymer electrolyte with high lithium ion conductivity for dendrite-free lithium metal batteries. *J. Mater. Chem. A* **2020**, *8*, 8033−8040.
(24) Zhu, Y.; Wang, F.; Liu, L.; Xiao, S.; Chang, Z.; Wu, Y. Composite of a nonwoven fabric with poly (vinylidene fluoride) as a gel membrane of high safety for lithium-ion battery. *Energy Environ. Sci.* **2013**, *6*, 618−624.
(25) Zhang, W.; Yi, Q.; Li, S.; Sun, C. An ion-conductive Li7La3Zr2O12-based composite membrane for dendrite-free lithium metal batteries. *J. Power Sources* **2020**, *450*, No. 227710.
(26) Gao, K.; Hu, X.; Dai, C.; Yi, T. Crystal structures of electrospun PVDF membranes and its separator application for rechargeable lithium metal cells. *Mater. Sci. Eng., B* **2006**, *131*, 100−105.
(27) Tarascon, J.; Gozdz, A.; Schmutz, C.; Shokoohi, F.; Warren, P. Performance of Bellcore's plastic rechargeable Li-ion batteries. *Solid State Ionics* **1996**, 8688−4954.
(28) Zhou, W.; Wang, S.; Li, Y.; Xin, S.; Manthiram, A.; Goodenough, J. Plating a Dendrite-Free Lithium Anode with a Polymer/Ceramic/Polymer Sandwich Electrolyte. *J. Am. Chem. Soc.* **2016**, *138*, 9385−9388.
(29) Zhu, M.; Wu, J.; Wang, Y.; Song, M.; Long, L.; Siyal, S.; Yang, X.; Sui, G. Recent advances in gel polymer electrolyte for high-performance lithium batteries. *J. Energy Chem.* **2019**, *37*, 126−142.
(30) Xu, D.; Su, J.; Jin, J.; Sun, C.; Ruan, Y.; Chen, C.; Wen, Z. In Situ Generated Fireproof Gel Polymer Electrolyte with $Li_{6.4}Ga_{0.2}La_3Zr_2O_{12}$ As Initiator and Ion-Conductive Filler. *Adv. Energy Mater.* **2019**, *9*, 1900611.
(31) Zhou, R.; Liu, W.; Yao, X.; Leong, Y. Poly (vinylidene fluoride) nanofibrous mats with covalently attached SiO_2 nanoparticles as an ionic liquid host: enhanced ion transport for electrochromic devices and lithium-ion batteries. *J. Mater. Chem. A* **2015**, *3*, 16040−16049.
(32) Chen, T.; Kong, W.; Zhang, Z.; Wang, L.; Hu, Y.; Zhu, G.; Chen, R.; Ma, L.; Yan, W.; Wang, Y.; Liu, J.; Jin, Z. Ionic liquid-immobilized polymer gel electrolyte with self-healing capability, high ionic conductivity and heat resistance for dendrite-free lithium metal batteries. *Nano Energy* **2018**, *54*, 17−25.
(33) Zhang, J.; Zhu, C.; Xu, J.; Wu, J.; Yin, X.; Chen, S.; Zhu, Z.; Wang, L. Enhanced mechanical behavior and electrochemical performance of composite separator by constructing crosslinked polymer electrolyte networks on polyphenylene sulfide nonwoven surface. *J. Mater. Chem. A* **2020**, *597*, No. 117622.
(34) Fan, L.; He, H.; Nan, C. Tailoring inorganic−polymer composites for the mass production of solid-state batteries. *Nat. Rev. Mater.* **2021**, *6*, 1003−1019.
(35) Zhao, C.; Zhang, X.; Cheng, X.; Zhang, R.; Xu, R.; Chen, P.; Peng, H.; Huang, J.; Zhang, Q. An anion-immobilized composite electrolyte for dendrite-free lithium metal anodes. *Proc. Natl. Acad. Sci.* **2017**, *114*, 11069.

https://doi.org/10.1021/acsomega.3c01258
ACS Omega 2023, 8, 16411−16418